Journal of Materials Chemistry A

Accepted Manuscript

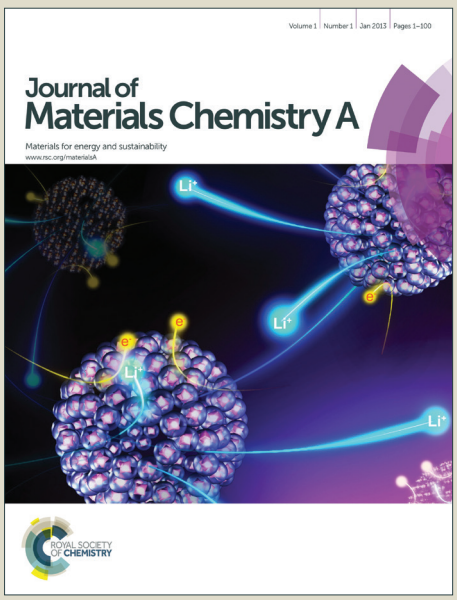

ROYAL SOCIETY OF CHEMISTRY

www.rsc.org/materialsA

Journal of Materials Chemistry A RSCPublishing

ARTICLE

4,4'-biphenyldicarboxylate sodium coordination compounds as an anode for Na-ion batteries

Aram Choi,[‡a], Yun Kyeong Kim[‡b], Tae Kyung Kim[b], Mi-Sook Kwon[a], Kyu Tae Lee*[a] and Hoi Ri Moon*[b]

Cite this: DOI: 10.1039/x0xx00000x

Received ooth January 2012,
Accepted ooth January 2012

DOI: 10.1039/x0xx00000x

www.rsc.org/

Novel 4,4'-biphenyldicarboxylate (bpdc) sodium salts with different compositions were evaluated for the first time as anodes for Na-ion batteries, and their crystal structures and corresponding electrochemical performances were analyzed. The structure of the bpdc-sodium salts was modified using precipitation and solvothermal methods to afford three different crystal structures with different degrees of deprotonation of the carboxylic acid (COOH) groups and different coordination of the water molecule, as determined by single crystal X-ray diffraction. The extent of deprotonation in bpdc-sodium salts not only affects their electrochemical performance, but also affects the corresponding reaction mechanisms. The fully deprotonated bpdc-disodium salt exhibits a promising electrochemical performance with a reversible capacity of about 200 mA h g^{-1} at ca. 0.5 V vs. Na/Na^+, stable cycle performance over 150 cycles, and an excellent rate performance of 100 mA h g^{-1} even at a 20 C rate, which are better than those of the partially deprotonated bpdc-sodium salt. The sodiation/desodiation of bpdc-sodium salts proceeds in a two-phase reaction, regardless of the degree of deprotonation. However, unlike the fully deprotonated bpdc-disodium salt, which shows a reversible phase transition during sodiation and desodiation, the partially deprotonated bpdc-sodium salt exhibits an irreversible phase transition during cycling.

1. Introduction

Sodium-ion batteries are considered a promising alternative for next-generation batteries that can replace Li-ion batteries in large-scale energy storage systems and electric vehicles, because of the potential cost advantages owing to the natural abundance of Na resources and geographically constrained Li resources.[1-6] A variety of electrode materials such as non-graphitic carbons,[7-9] alloys (e.g., Sn and Sb),[10-13] metal oxides,[14-18] and phosphorus [19, 20] have been shown to exhibit promising electrochemical performances as anodes for Na-ion batteries. Recently, a few organic compound-based materials such as conjugated and aromatic compounds containing carbonyl groups or *N*-heterocycles have been reported as promising anode materials because of their attractive features such as good electrochemical performance, low-cost production, recyclability, and structural diversity.[21-26] For example, organic electrode materials can be produced from commonly used recycled materials such as polyethylene terephthalate (PET). Several sodium terephthalate derivatives with amino- and bromo-groups have been easily synthesized owing to the structural diversity of organic architecture, resulting in controllable redox potential changes through inductive and resonance effects.[27] However, only a small number of organic compounds have been examined as electrode materials for rechargeable batteries such as Li-ion and Na-ion batteries.[28-37] In particular, only a few organic compounds have been examined as Na-ion batteries.[38-40]

[a] *School of Energy & Chemical Engineering*
Ulsan National Institute of Science and Technology (UNIST)
100 Banyeon-ri, Eonyang-eup, Ulju-gun, Ulsan, 689-798, South Korea
E-mail: ktlee@unist.ac.kr
[b] *School of Chemistry*
Ulsan National Institute of Science and Technology (UNIST)
100 Banyeon-ri, Eonyang-eup, Ulju-gun, Ulsan, 689-798, South Korea
E-mail: hoirimoon@unist.ac.kr

† Electronic Supplementary Information (ESI) available: Table of X-ray data and voltage profiles. See DOI: 10.1039/b000000x/

‡ These authors equally contributed.

Herein, we evaluated novel bpdc-sodium salts as anodes for Na-ion batteries for the first time, elucidated the correlation between the structural properties of organic anodes and those electrocemical performances. The bpdc-sodium salts were obtained using three different synthetic methods: precipitation at low and room temperatures, and solvothermal methods. Based on the degree of deprotonation of the carboxylic acid (COOH) groups and the coordination of water molecules, three different crystal structures for the bpdc-sodium salts were obtained. The crystal structures were determined and compared using single-crystal X-ray diffraction (XRD) and powder XRD (PXRD) patterns. The bpdc-sodium salts exhibit a promising electrochemical performance depending on the degree of deprotonation.

2. Experimental Section

Synthesis

$\{Na[Na(H_2O)](bpdc)\}_n$ (*hyd*-Na_2bpdc): To an aqueous suspension (3.2 mL) of 4,4'-biphenyldicarboxylic acid (H_2bpdc) (0.258 g, 1.06 mmol), an aqueous solution (0.8 mL) of NaOH (0.137 g, 3.43 mmol) was added. After the completion of the reaction, the solution was filtered, and the clear pale yellow filtrate was exposed to ethanol vapor inside a refrigerator (2 °C) to crystallize the products. After two days, block-shaped pale yellow single crystals of $\{Na[Na(H_2O)](bpdc)\}_n$ (*hyd*-Na_2bpdc) started to form at the surface of the solution. The crystals were filtered off after seven days, washed with ethanol, and dried in air. Yield: 0.17 g (53%). FT-IR (ATR): $\nu_{O\text{-}C=O(carboxylate)}$, 1579(s), 1390(s); $\nu_{O\text{-}H(coordinating\ water)}$ cm^{-1}. Anal. calcd for $Na_2C_{14}H_{10}O_5$ (304.21): C, 55.27; H, 3.31. Found: C, 53.26; H, 3.27.

$[(Na_2bpdc)]_n$ (Na_2bpdc): To a stirred aqueous suspension (25 mL) of 4,4'-biphenyldicarboxylic acid (2.42 g, 0.01 mol), an aqueous solution (7 mL) of NaOH (1.20 g, 0.03 mol) was added at room temperature. After the completion of the reaction, the solution was filtered, and ethanol (20 mL) was added to the filtrate, resulting in white precipitates. The white precipitate obtained was filtered, washed with ethanol, and dried in air. Yield: 2.04 g (71%). FT-IR (ATR): $\nu_{O\text{-}C=O}$, 1578(s), 1394(s) cm^{-1}. Anal. calcd for $Na_2C_{14}H_8O_4$ (286.19): C, 58.76; H, 2.82. Found: C, 57.48; H, 2.84.

$[NaHbpdc]_n$ (NaHbpdc): $NaNO_3$ (0.026 g, 0.30 mmol) was dissolved in methanol (2 mL) and H_2bpdc (0.036 g, 0.15 mmol) was dissolved in DMA/H_2O (5.1 mL, 4:1.1 *v/v*). The two solutions were placed in a glass jar and sealed together, and the mixture was heated at 100 ºC for 48 h. The solution was then cooled to room temperature. The plate-shaped colorless crystals obtained were filtered, washed briefly with methanol, and dried in air. Yield: 0.029 g (74%). FT-IR (ATR): $\nu_{C=O(carboxylic\ acid)}$, 1672 cm^{-1}; $\nu_{O\text{-}C=O(carboxylate)}$, 1605, 1399 cm^{-1}. Anal. calcd for $Na_1C_{14}H_9O_4$ (264.21): C, 63.64; H, 3.43. Found: C, 64.07; H, 3.88.

Characterization

All chemicals and solvents used in the syntheses were of reagent grade and they were used as received without further purification. The IR spectra were recorded using a ThermoFisher Scientific Nicolet 6700 FT-IR spectrophotometer. Elemental analyses (EA) were performed at the UNIST Central Research Facilities (UCRF) in Ulsan National Institute of Science and Technology (UNIST). Thermogravimetric analyses (TGA) were performed under N_2 (g) atmosphere at a scan rate of 5 °C/min using a Q50 (TA instruments). PXRD data were recorded using a Bruker D2 PHASER automated diffractometer at 30 kV and 10 mA for Cu Kα (λ = 1.54050 Å), with a step size of 0.02º in 2θ. Scanning electron microscopy was carried out using a cold FE-SEM (Hitachi). Single crystals of *hyd*-Na_2bpdc and NaHbpdc, coated with Paratone-N oil, were mounted on a loop, and the diffraction data were collected at 95 K with synchrotron radiation (λ = 0.64999 Å for *hyd*-Na_2bpdc; 0.69999 Å for NaHbpdc) using a ADSC Quantum-210 detector at 2D SMC with a silicon (111) double crystal monochromator (DCM) at Pohang Accelerator Laboratory, S. Korea. The ADSC Q210 ADX program was used for the data collection, and HKL3000 (Ver. 703r) was used for the cell refinement, reduction, and absorption correction. The structures of *hyd*-Na_2bpdc and NaHbpdc have been deposited in the CCDC database, reference numbers 944127 and 944128, respectively.

Electrochemical measurements

The samples of electrochemically active materials (57.1 wt%) were mixed with carbon black (Super P, 28.6 wt%) and carboxymethyl cellulose (CMC, 14.3 wt%). The loading amount of electrode materials is about 1 mg cm^{-2}. The electrochemical performance was evaluated using 2032 coin cells with a Na metal anode and 0.8 M $NaClO_4$ in a mixture of ethylene carbonate and diethyl carbonate (1:1 v/v) electrolyte solution. The galvanostatic experiments were performed at 30°C, and specific current densities of 18.7 mA g^{-1} (ca. 0.1 C) and 20.3 mA g^{-1} (ca. 0.1 C) were applied to evaluate the cycle performances of NaHbpdc and Na_2bpdc, respectively. For the rate performance evaluation, the discharging (desodiation) current density was fixed at 0.1 C, and the charging current was varied. The GITT experiments were performed between 0.1 and 2.5 V vs. Na/Na^+ by applying a current corresponding to a C/20 rate in intervals of 1 h, separated by a rest period of 1 h. The electrochemical impedance spectroscopy (EIS) study was performed using a BIO Logic SP 150. The AC impedance measurements were recorded using a signal with amplitude of 5 mV and a frequency range from 300 kHz to 1 mHz.

3. Results and Discussion

H_2bpdc ligand and sodium cations were reacted under three different reaction conditions to afford three different types of bpdc-sodium salts. Disodium bpdc monohydrate (*hyd*-Na_2bpdc), $\{Na[Na(H_2O)](bpdc)\}_n$, was synthesized by the reaction of NaOH with H_2bpdc in water, and single crystals of the product were obtained by slow diffusion of ethanol at ca. 2 °C. NaOH was employed in this reaction as a source of Na ions and a strong base for deprotonating the carboxylic acid (COOH) groups of H_2bpdc. On the other hand, interestingly, non-hydrated disodium bpdc (Na_2bpdc) was synthesized as a microcrystalline solid by the rapid reaction of NaOH with H_2bpdc in a mixture of water and

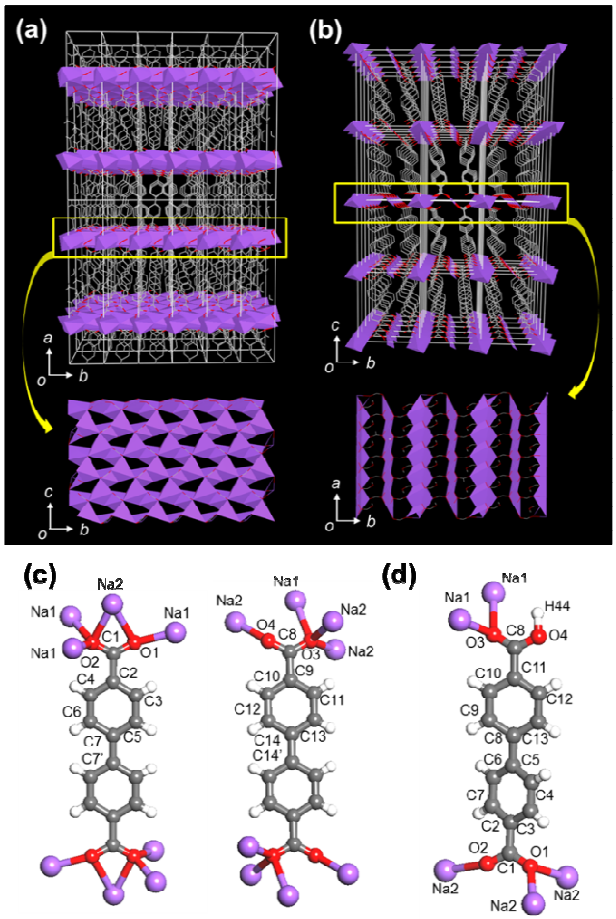

Fig. 1 Single-crystal X-ray structures of *hyd*-Na_2bpdc and NaHbpdc, which were constructed by connecting the SBUs (purple) by $bpdc^{2-}$ ligands. 3D network of (a) *hyd*-Na_2bpdc and (b) NaHbpdc; coordination modes of $bpdc^{2-}$ ligands to sodium ions in (c) *hyd*-Na_2bpdc, and (d) NaHbpdc. Color scheme: C (grey), O (red), H (white), Na (purple).

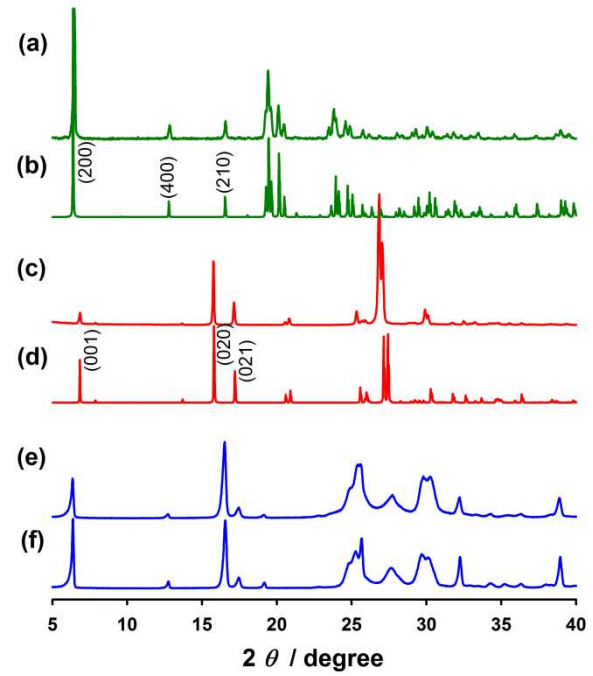

Fig. 2 PXRD patterns of (a) *hyd*-Na_2bpdc and (c) NaHbpdc, simulated patterns from single-crystal XRD data of (b) *hyd*-Na_2bpdc and (d) NaHbpdc, and PXRD patterns of (e) Na_2bpdc and (f) dehydrated *hyd*-Na_2bpdc dried at 120 °C.

ethanol at room temperature. The partially deprotonated sodium salt, monosodium bpdc (NaHbpdc), $[Na(Hbpdc)]_n$, was synthesized by the solvothermal reaction of $NaNO_3$ and H_2bpdc in a mixture of methanol, *N,N*-dimethylacetamide (DMA), and water at 100 °C. Under these conditions, only one of two carboxylic acid (COOH) groups of H_2bpdc was deprotonated. Thus, the three bpdc-sodium salts were composed of the same organic (bpdc) and inorganic (Na^+) building blocks, but had different compositions and crystal structures.

Because *hyd*-Na_2bpdc and NaHbpdc could be obtained as single crystals, their crystal structures were directly determined and compared via single-crystal X-ray diffraction results. The lattice parameters, agreement factors, and detailed structural information of *hyd*-Na_2bpdc and NaHbpdc are listed in Table S1. *hyd*-Na_2bpdc crystallized in the monoclinic $P2_1/c$ space group. As shown in Fig. 1a, the structure of *hyd*-Na_2bpdc consisted of Na-O layers as the secondary building units (SBUs), and the bridging ligands, $bpdc^{2-}$, formed a three-dimensional (3D) network. The Na-O layers resulted from the coordination between Na^+ ions and O atoms of carboxylate groups (COO^-) and water molecules. The crystal structure of *hyd*-Na_2bpdc possessed two Na^+, two halves of $bpdc^{2-}$ ligand, and one coordinating water molecule, which are crystallographically independent. Fig. 1c reveals the coordination modes of carboxylates (COO^-) in *hyd*-Na_2bpdc to be as follows: the O1-C1-O2 group acts as a tetradentate ligand forming a four-membered chelate ring, and the O3-C8-O4 group coordinates to four Na ions without chelation. Na1 and Na2 exhibited a distorted trigonal bipyramidal and an octahedral coordination geometry, respectively. The $bpdc^{2-}$ ligand was planar with a dihedral angle of 0° between the two phenyl rings.

NaHbpdc crystallized in the triclinic P-*1* space group. The crystal structure of NaHbpdc showed two crystallographycally independent Na^+ ions and one $bpdc^{2-}$ ligand. The Na^+ ions were bridged by carboxylate groups (COO^-) to form one-dimensional (1D) Na-O chains as SBUs, which were linked by $bpdc^{2-}$ ligands to form a 3D network (Fig. 1b). Na1 and Na2 showed distorted octahedral and square planar geometry, respectively. Unlike *hyd*-Na_2bpdc, the phenyl rings in the $bpdc^{2-}$ ligand of NaHbpdc were tilted by 30.69(5)°. Because the carboxylic acid (COOH) groups in NaHbpdc were partially depronated, the deprotonated O1-C1-O2 group coordinated to three Na ions using both the oxygen atoms. In contrast, only the O3 atom in O3-C8-O4-H44 acted as a bidentate ligand (Fig. 1d).

The PXRD patterns of the as-synthesized *hyd*-Na_2bpdc and NaHbpdc powders were compared to the simulated patterns based on the single crystal XRD data, respectively. As shown in Figs. 2a-d, the XRD patterns of both the bulk powders showed good agreement with the corresponding simulated patterns, indicating that the phase pure powders have the same crystal structure as the single crystals. On the other hand, because Na_2bpdc was obtained as microcrystals, which are not suitable for single crystal XRD analysis, its PXRD pattern (Fig. 2e) was compared to those of

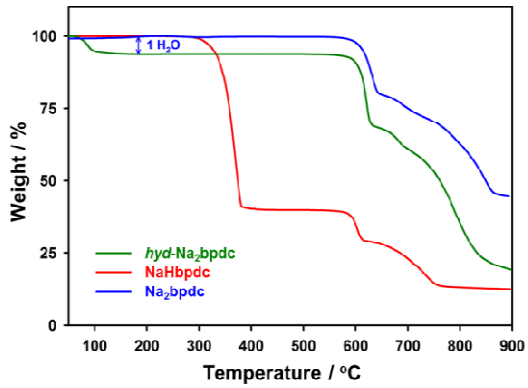

Fig. 3 TGA curves of *hyd*-Na_2bpdc, NaHbpdc, and Na_2bpdc.

hyd-Na_2bpdc and NaHbpdc. Na_2bpdc showed a different PXRD pattern, indicating that the crystal structure of Na_2bpdc was different from those of *hyd*-Na_2bpdc and NaHbpdc. However, the structure of Na_2bpdc was found to be the same as that of *hyd*-Na_2bpdc after the coordinating water molecules were removed (Fig. 2f). *hyd*-Na_2bpdc was dehydrated by heating at 120 °C under vacuum. The dehydration results in a weight loss of 5.98% below 100 °C in the thermogravimetric analysis (TGA) curves of *hyd*-Na_2bpdc (Fig. 3). The amount of weight loss corresponded to one water molecule per molecular formula. The incorporation of water molecules in the structure of Na_2bpdc may depend on the reaction temperature as well as the type of solvent used.

Further, the structural similarity between *hyd*-Na_2bpdc and Na_2bpdc is indirectly supported by the TGA curves because they show the same thermal behavior except for the water loss in *hyd*-Na_2bpdc below 100 °C (Fig. 3). Although both *hyd*-Na_2bpdc and Na_2bpdc are decomposed at ca. 600 °C, Na_2bpdc did not show any weight loss around 100 °C indicating that this compound is not hydrated. On the other hand, NaHbpdc exhibited no weight loss around 100 °C, which is consistent with the single-crystal XRD data of NaHbpdc, which is not hydrated. The structure of NaHbpdc is rapidly decomposed above 300 °C. The lower thermal stability of NaHbpdc compared to *hyd*-Na_2bpdc and Na_2bpdc is attributed to the weak coordination between Na^+ ions

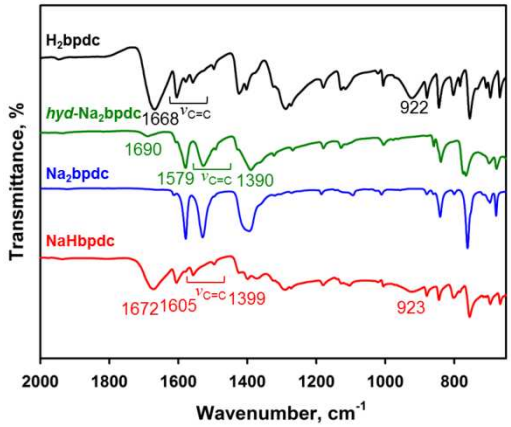

Fig. 4 FT-IR spectra of H_2bpdc, *hyd*-Na_2bpdc, Na_2bpdc and NaHbpdc; all the spectra were measured by using attenuated total reflectance (ATR) technique.

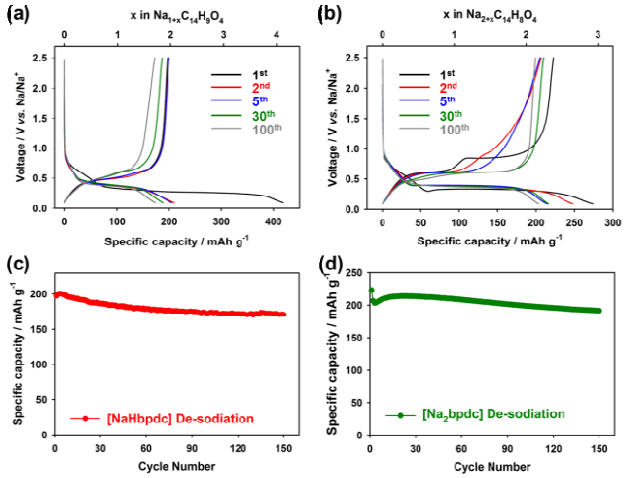

Fig. 5 Voltage profiles of (a) NaHbpdc and (b) Na_2bpdc; cycle performance of (c) NaHbpdc and (d) Na_2bpdc.

and the carbonyl group of carboxylic acid (COOH) groups, which were not deprotonated. This indicates that a higher degree of deprotonation is required to improve the thermal stability of organic electrode materials.

The acid-base reactions of H_2bpdc with sodium precursors to produce *hyd*-Na_2bpdc, Na_2bpdc and NaHbpdc were further verified by Fourier Transform infrared (FT-IR) spectroscopy. As shown in Fig. 4, the spectrum of H_2bpdc showed typical C=O stretching and O-H bending vibrations of carboxylic acid (COOH) groups at 1668 and 922 cm^{-1}, respectively. However, after the formation of the metal-carboxylate coordination (COO-Na) compounds via complete deprotonation by NaOH, the carbonyl (C=O) stretching vibration of the carboxylate groups (COO^-) in *hyd*-Na_2bpdc was shifted and split into two bands at 1579 and 1390 cm^{-1}, which were assigned as asymmetric (ν_{as}) and symmetric (ν_s) stretching vibrations, respectively (Fig. 4). Moreover, the characteristic O-H bending vibrations for the carboxylic acid groups around 920 cm^{-1} disappeared. The weak peak at 1690 cm^{-1} in the spectrum of *hyd*-Na_2bpdc corresponds to the O-H bending vibration of water. This observation agrees with the existence of guest water molecules, as suggested by single-crystal XRD and TGA data. Na_2bpdc showed the same FT-IR spectrum as *hyd*-Na_2bpdc, except for the peak around 1690 cm^{-1}. As expected from the XRD and TGA results, the FT-IR spectrum of NaHbpdc, containing both of the protonated and deprotonated form of carboxylic acid groups, showed peaks characteristic of both COOH and COO^- groups, i.e., C=O stretching and O-H bending vibrations of carboxylic acid at 1672 and 923 cm^{-1}, respectively, and ν_{as} and ν_s of the carboxylate groups at 1605 and 1399 cm^{-1}, respectively (Fig. 4).

As shown in Fig. 5, Na_2bpdc and NaHbpdc, which have different crystal structures and degrees of deprotonation of the organic ligands, were examined as anode materials for Na-ion batteries. The cycle performance of *hyd*-Na_2bpdc was not examined separately because it transforms into Na_2bpdc during the preparation of the electrodes. The electrodes were dried at 120 °C under vacuum to remove the adsorbed water molecules on the surface of powders that is related to electrolyte decomposition during charging/discharging. This drying process leads to the

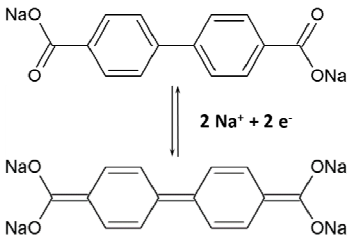

Scheme 1 Schematic diagram for the electrochemical redox reaction mechanism of Na_2bpdc.

dehydration of *hyd*-Na_2bpdc to afford Na_2bpdc. Both Na_2bpdc and NaHbpdc electrodes showed similar reversible capacities of approximately 200 mA h g^{-1} at ca. 0.5 V vs. Na/Na^+, which is larger than the theoretical specific capacity of 187 mA h g^{-1} corresponding two Na^+ ions storage, as shown in Scheme 1. The excess capacity (about 30 mA h g^{-1}) is attributed to carbon additive (super P) that can reversibly store Na^+ ions and delivers about 100 mA h g^{-1} (Fig. S2). The gravimetric specific capacity of bpdc-sodium salts is relatively small compared to other anode materials. Moreover, the densities of Na_2bpdc and NaHbpdc are 1.566 g cm^{-3} and 1.657 g cm^{-3}, respectively, based on X-ray single crystallographic data, which causes a low volumetric energy density. However, these organic electrode materials are inexpensive, indicating that organic electrode materials have an advantage of low cost/energy density. Above all, organic electrode materials are environmentally benign and reproducible, and this makes organic electrode materials attractive in spite of their relatively low energy density. Also, they showed a stable cycle performance over 150 cycles. Notably, unlike Na_2bpdc, NaHbpdc showed a large amount of irreversible capacity at the first cycle. The coulombic efficiencies of Na_2bpdc and NaHbpdc at the first cycle were 81% and 47%, respectively. The poor coulombic efficiency of NaHbpdc (large sodiation capacity at the first cycle) is attributed to its irreversible electrolyte decomposition on the surface of NaHbpdc possessing carboxylic acid groups. The same behavior, i.e., a large amount of irreversible capacity at the first cycle, was also observed in a partially deprotonated monosodium terephthalate,[39] while a fully deprotonated disodium terephatalate showed good coulombic efficiency similar to Na_2bpdc.

The rate performances of Na_2bpdc and NaHbpdc were also compared, as shown in Figs. 6 and S1. Na_2bpdc showed a better rate performance than NaHbpdc, and even at a 20 C rate (3.74 A g^{-1}), Na_2bpdc sustained 50% of reversible capacity delivered at a 0.2 C rate. This superior rate performance of Na_2bpdc is definitely attributed to the smaller particle size (diffusion length) of Na_2bpdc compared to NaHbpdc, as shown in Fig. 7. The particle sizes of Na_2bpdc and NaHbpdc are a few μm and approximately 10 μm, respectively. However, even the dehydrated *hyd*-Na_2bpdc, which has a size similar to NaHbpdc, exhibited a better rate performance than NaHbpdc, indicating that the rate performance is affected by both the degree of deprotonation and the particle size of the bpdc-sodium salts. Note that little change of particle sizes of NaHbpdc and Na_2bpdc was observed after water-treatment at the same condition of electrode preparation, because only a very small amount of water was used

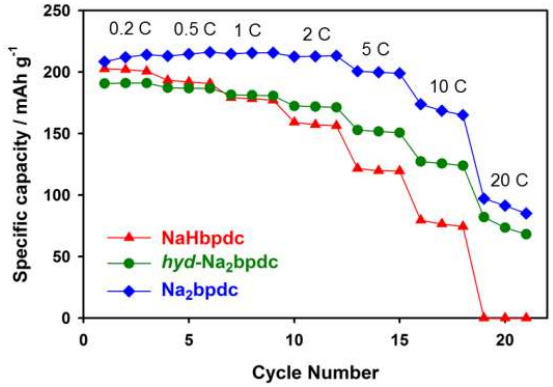

Fig. 6 Rate performance of *hyd*-Na_2bpdc, Na_2bpdc and NaHbpdc.

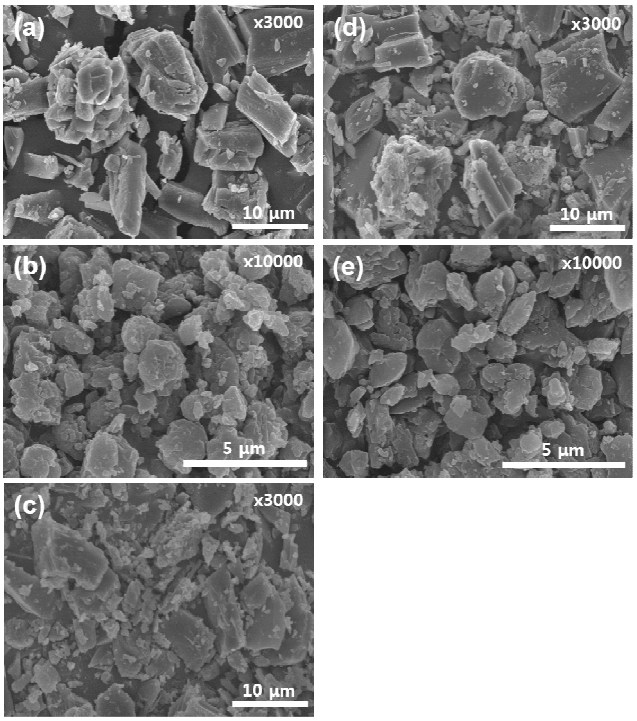

Fig. 7 SEM images of bare (a) NaHbpdc, (b) Na_2bpdc, and (c) *hyd*-Na_2bpdc powders, and water-treated (d) NaHbpdc and (e) Na_2bpdc powders at the same condition of electrode preparation.

for the electrode preparation despite of that they are slightly soluble in water, indicating that the particle sizes of NaHbpdc and Na_2bpdc were not changed after the electrode preparation.

Electrodes with carboxylic acid groups cause a large amount of electrolyte decomposition, forming thick solid electrolyte interphase (SEI) layers, which result in the increase in polarization because of a large charge-transfer resistance. This is supported by the electrochemical impedance spectroscopy (EIS) analysis. The measurement was performed using the symmetric cells comprised of the same working electrode (bpdc salt) / working electrode (bpdc salt). The working electrodes were half-sodiated charging state after pre-cycling. As shown in Fig. 8, the semicircle of NaHbpdc is larger than that of *hyd*-Na_2bpdc, indicating that the charge-transfer resistance of NaHbpdc is larger than that of *hyd*-Na_2bpdc because the semicircle corresponds to charge-transfer resistance that is dependent on SEI layers. Also,

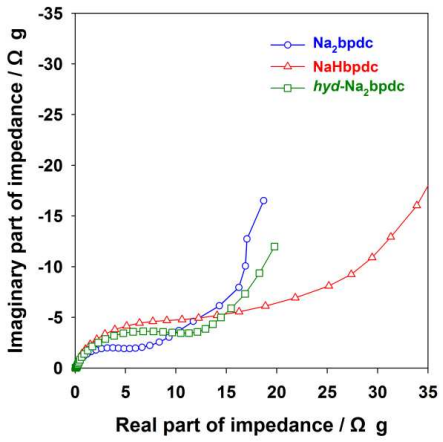

Fig. 8 Nyquist plots of bpdc electrode/bpdc electrode symmetric cells

the smaller charge-transfer resistance of Na_2bpdc than *hyd*-Na_2bpdc is attributed to the larger surface area cuased by smaller particle size. Moreover, while both the Na^+ cations present in the structure of Na_2bpdc can act as charge carriers for the solid state diffusion of Na^+ ions, the proton present in the structure of NaHbpdc cannot act as a charge carrier because it is strongly bound to the carbonyl group through covalent bonding. This indicates that the reduced amount of charge carriers in NaHbpdc compared to Na_2bpdc causes slower ionic diffusivity of Na^+ ions, resulting in poorer rate performance.

To observe the structural changes upon sodiation/desodiation, *ex situ* XRD analysis of Na_2bpdc was performed, and it showed that the reversible sodiaiton/desodiation of Na_2bpdc proceeds in a two-phase reaction, as shown in Fig. 9. Upon sodiation, the intensity of PXRD peaks corresponding to Na_2bpdc decreased, and new peaks corresponding to the sodiated phase of Na_2bpdc gradually appeared at ca. 11, 20, 23 and 31° (and vice versa for the desodiation). Despite two plateau steps in the voltage profile of desodiation during the first cycle, the *ex situ* XRD patterns showed that only one type of a two-phase reaction occurred during the desodiation. This agrees well with the galvanostatic intermittent titration technique (GITT) curves, as shown in Fig. 10. Although two plateaus were observed during the first cycle, the second plateau is attributed to larger polarization because of a higher mass transfer resistance in Na-deficient compositions. This type of polarization behavior gradually disappeared on cycling, and may be closely related to the amorphization of Na_2bpdc during the cycling. As shown in the *ex situ* XRD patterns of the electrodes during cycling (Fig. 9c), broader PXRD peaks were observed after the cycling, indicating that the amorphization of Na_2bpdc occurred during cycling. In general, materials that are more amorphous show less polarization owing to the faster ionic diffusion at grain boundaries.

Unlike Na_2bpdc, NaHbpdc showed an the irreversible phase transformation during the sodiation and desodiation, as shown in Fig. 11. NaHbpdc proceeds in a two-phase reaction during the sodiation and desodiation; however, the mixture phases of NaHbpdc and Na_2bpdc were observed after the desodiation. This indicates that the ion exchange occurred between the proton of carboxylic acid group in NaHbpdc and sodium ions in electrolytes during cycling. Similar behavior has been observed

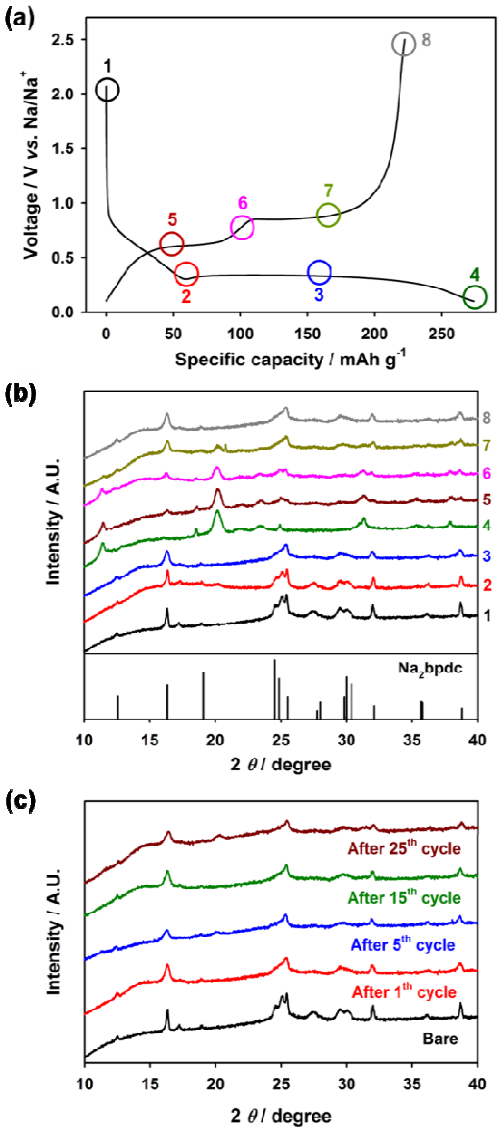

Fig. 9 *Ex situ* XRD analysis of Na_2bpdc: (a) voltage profiles, (b) corresponding XRD patterns, and (c) XRD patterns of desodiated electrodes during the various cyclings.

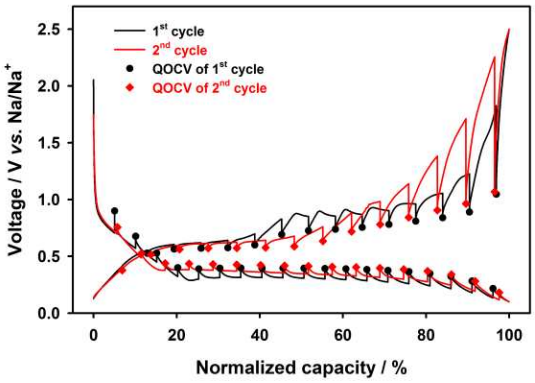

Fig. 10 GITT curves of Na_2bpdc.

in the partially deprotonated monosodium terephthalate, which was transformed into the fully deprotonated disodium terephthalate due to the ion exchange between the proton and

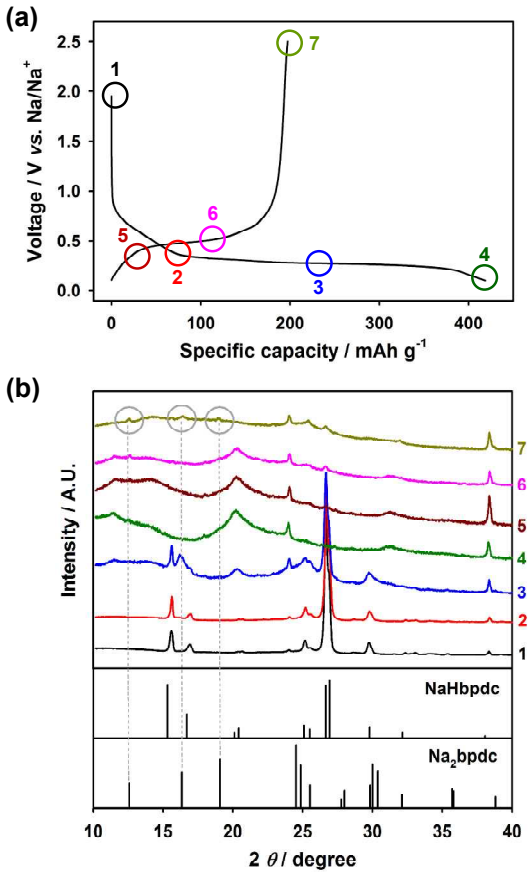

Fig. 11 *Ex situ* XRD analysis of NaHbpdc: (a) voltage profiles and (b) corresponding XRD patterns.

sodium during sodiation and desodiation.[39] The ion exchange of NaHbpdc powders was not observed when NaHbpdc powders were stored in electrolytes for 3, 5, and 10 days without passage of current, as shown in Fig. S3, and thus, the ion exchange is merely related to electrochemical sodiation and desodiation. The ion-exchange behaviour of NaHbpdc on cycling is further supported by the comparison between the differential capacity (dQ/dV) plots of NaHbpdc and Na_2bpdc. As the cycle number increases, the intensity of oxidative peaks of NaHbpdc at 0.5 V and 0.6 V vs. Na/Na^+ decreases and increases, respectively (Fig. 12a). The oxidative peak at 0.6 V corresponds to the oxidative peak of Na_2bpdc, as observed in the dQ/dV plots of Na_2bpdc (Fig. 12b). Therefore, this indicates that some of NaHbpdc was transformed into Na_2bpdc during cycling.

4. Conclusions

In conclusion, the crystal structures and electrochemical performance of bpdc-sodium salts as anode materials for Na-ion batteries have been evaluated for the first time. The different degrees of deprotonation and differently coordinated water molecules in the bpdc-sodium salts were obtained through deliberate synthesis such as precipitation and solvothermal methods, resulting in the formation of bpdc-sodium salts with three different crystal structures. Their crystal structures were

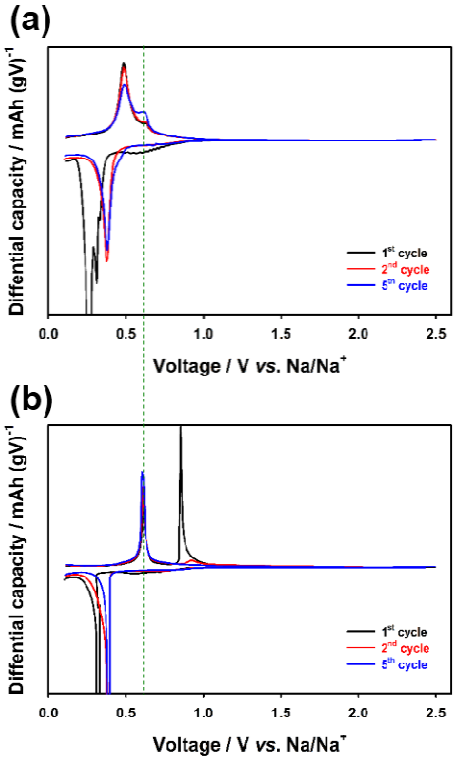

Fig. 12 Differential capacity (dQ/dV) plots of (a) NaHbpdc and (b) Na_2bpdc electrodes.

determined using single-crystal XRD. The bpdc-sodium salts exhibited a promising electrochemical performance with a reversible capacity of 220 mA h g^{-1} at ca. 0.5 V vs. Na/Na^+, negligible capacity fading over 150 cycles, and an excellent rate performance of approximately 100 mA h g^{-1} even at a 20 C rate. The sodiation/desodiation of bpdc-sodium salts proceeds in a two-phase reaction. In addition, the degree of deprotonation in bpdc-sodium salts not only affected the electrochemical performance, but also affected the corresponding reaction mechanisms. The fully deprotonated bpdc-disodium salt (Na_2bpdc) showed better coulombic efficiency and rate performance than the partially deprotonated bpdc-monosodium salt (NaHbpdc). Unlike Na_2bpdc, which showed reversible phase transition during sodiation and desodiation, NaHbpdc exhibited an irreversible phase transition during the cycling.

Acknowledgements

We acknowledge financial support from the Korea CCS R&D Center (KCRC) grant funded by the Korea government (Ministry of Science, ICT & Future Planning) (NRF-2013M1A8A1039968). This research was also partly supported by the National Research Foundation of Korea (NRF) grant funded by the Korea Government (MEST) (No. 2010-0019408 and No. NRF-2013R1A1A2013446), and by the year of 2010 Research Fund of the UNIST(Ulsan National Institute of Science and Technology).

Notes and references

1. B. L. Ellis and L. F. Nazar, *Curr. Opin. Solid State Mat. Sci.*, 2012, **16**, 168.
2. V. Palomares, M. Casas-Cabanas, E. Castillo-Martinez, M. H. Han and T. Rojo, *Energ Environ. Sci*, 2013, **6**, 2312.
3. H. L. Pan, Y. S. Hu and L. Q. Chen, *Energy Environ. Sci.*, 2013, **6**, 2338.
4. S. Y. Hong, Y. Kim, Y. Park, A. Choi, N. S. Choi and K. T. Lee, *Energy Environ. Sci.*, 2013, **6**, 2067.
5. S. W. Kim, D. H. Seo, X. H. Ma, G. Ceder and K. Kang, *Adv. Energy Mater.*, 2012, **2**, 710.
6. M. D. Slater, D. Kim, E. Lee and C. S. Johnson, *Adv. Funct. Mater.*, 2013, **23**, 947.
7. Y. Y. Shao, J. Xiao, W. Wang, M. Engelhard, X. L. Chen, Z. M. Nie, M. Gu, L. V. Saraf, G. Exarhos, J. G. Zhang and J. Liu, *Nano Lett.*, 2013, **13**, 3909.
8. S. Komaba, W. Murata, T. Ishikawa, N. Yabuuchi, T. Ozeki, T. Nakayama, A. Ogata, K. Gotoh and K. Fujiwara, *Adv. Funct. Mater.*, 2011, **21**, 3859.
9. Y. L. Cao, L. F. Xiao, M. L. Sushko, W. Wang, B. Schwenzer, J. Xiao, Z. M. Nie, L. V. Saraf, Z. G. Yang and J. Liu, *Nano Lett.*, 2012, **12**, 3783.
10. Y. H. Xu, Y. J. Zhu, Y. H. Liu and C. S. Wang, *Adv. Energy Mater.*, 2013, **3**, 128.
11. A. Darwiche, C. Marino, M. T. Sougrati, B. Fraisse, L. Stievano and L. Monconduit, *J. Am. Chem. Soc.*, 2012, **134**, 20805.
12. L. Baggetto, E. Allcorn, A. Manthiram and G. M. Veith, *Electrochem. Commun.*, 2013, **27**, 168.
13. H. L. Zhu, Z. Jia, Y. C. Chen, N. Weadock, J. Y. Wan, O. Vaaland, X. G. Han, T. Li and L. B. Hu, *Nano Lett.*, 2013, **13**, 3093.
14. Y. S. Wang, X. Q. Yu, S. Y. Xu, J. M. Bai, R. J. Xiao, Y. S. Hu, H. Li, X. Q. Yang, L. Q. Chen and X. J. Huang, *Nature commun.*, 2013, **4**.
15. P. Senguttuvan, G. Rousse, V. Seznec, J. M. Tarascon and M. R. Palacin, *Chem. Mat.*, 2011, **23**, 4109.
16. Q. Sun, Q. Q. Ren, H. Li and Z. W. Fu, *Electrochem. Commun.*, 2011, **13**, 1462.
17. Y. Sun, L. Zhao, H. L. Pan, X. Lu, L. Gu, Y. S. Hu, H. Li, M. Armand, Y. Ikuhara, L. Q. Chen and X. J. Huang, *Nature commun.*, 2013, **4**.
18. S. H. Woo, Y. Park, W. Y. Choi, N. S. Choi, S. Nam, B. Park and K. T. Lee, *J. Electrochem. Soc.*, 2012, **159**, A2016.
19. Y. Kim, Y. Park, A. Choi, N. S. Choi, J. Kim, J. Lee, J. H. Ryu, S. M. Oh and K. T. Lee, *Adv. Mater.*, 2013, **25**, 3045.
20. J. F. Qian, X. Y. Wu, Y. L. Cao, X. P. Ai and H. X. Yang, *Angew. Chem. Int. Ed.*., 2013, **52**, 4633.
21. Y. Liang, Z. Tao and J. Chen, *Adv. Energy Mater.*, 2012, **2**, 742.
22. M. Armand, S. Grugeon, H. Vezin, S. Laruelle, P. Ribiere, P. Poizot and J. M. Tarascon, *Nature mater.*, 2009, **8**, 120.
23. J. Geng, J.-P. Bonnet, S. Renault, F. Dolhem and P. Poizot, *Energy Environ. Sci.*, 2010, **3**, 1929.
24. X. Han, G. Qing, J. Sun and T. Sun, *Angew. Chem. Int. Ed.*, 2012, **51**, 5147.
25. Y. Liang, P. Zhang and J. Chen, *Chem. Sci.*, 2013, **4**, 1330.
26. Y. Morita, S. Nishida, T. Murata, M. Moriguchi, A. Ueda, M. Satoh, K. Arifuku, K. Sato and T. Takui, *Nature mater.*, 2011, **10**, 947.
27. Y. Park, D. S. Shin, S. H. Woo, N. S. Choi, K. H. Shin, S. M. Oh, K. T. Lee and S. Y. Hong, *Adv. Mater.*, 2012, **24**, 3562.
28. B. Genorio, K. Pirnat, R. Cerc-Korosec, R. Dominko and M. Gaberscek, *Angew. Chem. Int. Ed.*, 2010, **49**, 7222.
29. X. Han, F. Yi, T. Sun and J. Sun, *Electrochem. Commun.*, 2012, **25**, 136.
30. S. Nishida, Y. Yamamoto, T. Takui and Y. Morita, *ChemSusChem*, 2013, **6**, 794.
31. Z. Song, H. Zhan and Y. Zhou, *Angew. Chem. Int. Ed.*, 2010, **49**, 8444.
32. W. Walker, S. Grugeon, O. Mentre, S. Laruelle, J.-M. Tarascon and F. Wudl, *J. Am. Chem. Soc.*, 2010, **132**, 6517.
33. W. Xu, A. Read, P. K. Koech, D. Hu, C. Wang, J. Xiao, A. B. Padmaperuma, G. L. Graff, J. Liu and J.-G. Zhang, *J. Mater. Chem.*, 2012, **22**, 4032.
34. M. Yao, H. Senoh, S.-i. Yamazaki, Z. Siroma, T. Sakai and K. Yasuda, *J. Power Sources*, 2010, **195**, 8336.
35. A. L. Reddy, S. Nagarajan, P. Chumyim, S. R. Gowda, P. Pradhan, S. R. Jadhav, M. Dubey, G. John and P. M. Ajayan, *Sci. rep.*, 2012, **2**, 960.
36. C. Luo, R. Huang, R. Kevorkyants, M. Pavanello, H. He and C. Wang, *Nano Lett.*, 2014, **14**, 1596.
37. C. Luo, Y. Zhu, Y. Xu, Y. Liu, T. Gao, J. Wang and C. Wang, *J. Power Sources*, 2014, **250**, 372.
38. L. Zhao, J. M. Zhao, Y. S. Hu, H. Li, Z. B. Zhou, M. Armand and L. Q. Chen, *Adv. Energy Mater.*, 2012, **2**, 962.
39. A. Abouimrane, W. Weng, H. Eltayeb, Y. J. Cui, J. Niklas, O. Poluektov and K. Amine, *Energy Environ. Sci.*, 2012, **5**, 9632.
40. K. Sakaushi, E. Hosono, G. Nickerl, T. Gemming, H. Zhou, S. Kaskel and J. Eckert, *Nature commun.*, 2013, **4**, 1485.